

## Valence Auger decay following $3s$ photoionization in potassium

J. Palaudoux,<sup>1,2</sup> S. Sheinerman,<sup>3</sup> J. Soronen,<sup>4</sup> S.-M. Huttula,<sup>4</sup> M. Huttula,<sup>4</sup> K. Jänkälä,<sup>4</sup> L. Andric,<sup>1,2</sup> K. Ito,<sup>1,2,5</sup> P. Lablanquie,<sup>1,2</sup> F. Penent,<sup>1,2</sup> J.-M. Bizau,<sup>5,6</sup> S. Guilbaud,<sup>6</sup> and D. Cubaynes<sup>5,6</sup>

<sup>1</sup>*Sorbonne Universités, UPMC, Université Paris 06, Laboratoire de Chimie Physique-Matière et Rayonnement, 11 rue Pierre et Marie Curie, 75231 Paris Cedex 05, France*

<sup>2</sup>*CNRS, LCPMR (UMR 7614), 11 rue Pierre et Marie Curie, 75231 Paris Cedex 05, France*

<sup>3</sup>*Department of Physics, St. Petersburg State Maritime Technical University, 198262 St. Petersburg, Russia*

<sup>4</sup>*MOMA-RC, P.O. Box 3000, 90014 University of Oulu, Finland*

<sup>5</sup>*Synchrotron SOLEIL, l'Orme des Merisiers, Saint-Aubin, BP 48, 91192 Gif-sur-Yvette Cedex, France*

<sup>6</sup>*ISMO, CNRS UMR 8214, Université Paris-Sud, Bâtiment 350, F-91405 Orsay Cedex, France*

(Received 21 April 2015; published 10 July 2015)

We have studied photoionization in the inner valence  $3s$  subshell of K and the spectroscopic properties of the two  $3s^{-1}$  ( $^1S$ ) and ( $^3S$ ) resulting states. Similar to the Rb and Cs cases, the lifetime widths of the ( $^1S$ ) and ( $^3S$ ) states are found to be markedly different, due to the electron correlation effects. The main part of the study deals with the subsequent Auger decay of the  $3s^{-1}$  states, which have the particularity to involve low energy ( $\sim 5$  eV) Auger electrons. A magnetic bottle spectrometer with a multicoincidence technique has been used to observe and filter the Auger spectra with respect to the  $K^{2+}$  final state. The evolution of these Auger spectra has been investigated near the ionization threshold. They show strong post-collision interaction (PCI) effects, which are well reproduced by semiclassical and eikonal models. They reveal the importance of the photoelectron–Auger-electron interaction associated with these low energy Auger electrons.

DOI: [10.1103/PhysRevA.92.012510](https://doi.org/10.1103/PhysRevA.92.012510)

PACS number(s): 31.15.V-, 32.30.-r, 32.70.Jz, 32.80.Hd

### I. INTRODUCTION

Alkali-metal atoms are neighbors of rare gas atoms in the periodic table. Their electronic configuration is similar to rare gases except for an extra outer shell  $(n + 1)s$  electron: compare electronic configurations of neon Ne and sodium Na = [Ne] $3s$  or argon Ar and potassium K = [Ar] $4s$ . This suggests that some similar physical properties can be expected, but also notable and interesting differences. In this paper we want to address the fate of the ionization in the inner valence  $ns$  shell, and more specifically of the  $3s$  inner valence shell in K. As their outer  $(n + 1)s$  electron is easily ionized, alkali-metal atoms present low single and double ionization potentials. For K, they are respectively 4.3407 and 35.9656 eV [1]. A consequence is that, contrary to rare gases, the inner valence  $ns^{-1}$  holes in alkali-metal atoms can decay by emission of an Auger electron. Another difference is that while  $ns^{-1}$  holes in rare gases correspond to a single  $^2S$  electronic term, in alkali-metal atoms they give rise to two electronic terms ( $^1S$ ) and ( $^3S$ ), which reflect the spin coupling between the remaining  $ns$  inner valence electron and the outer  $(n + 1)s$  electron. We have here the interesting situation that two close electronic states decay by emission of low energy Auger electrons ( $\sim 5$  eV in K).

Photoionization in the valence  $ns$  shell is documented in other alkali-metal atoms: Richter *et al.* [2] reported  $2s$  photoionization of Na in its ground state and in its laser excited [Ne] $3p$  configuration. Similar studies were performed more recently for the  $4s$  inner valence photoionization in Rb [3] and the  $5s$  in Cs [4] in their ground and laser excited states. Indirect experimental information exists on the  $K^+ 3s^{-1}$  states: for instance resonances resulting from the  $3s$  excitation to empty orbitals were observed in ion yields [5,6] and the Auger decay of the  $K^+ 3s^{-1}$  ( $^1S$ ) state was observed in  $K^+$ -He collisions [7].  $K^+ 3s^{-1}$  cross sections were calculated by Kupliauskienė [8]. However, to the best of our knowledge, no direct experiment

has been reported on the  $3s$  photoionization of K atom, even in its ground state. The first objective of this work is thus to present data for the binding energy, lifetime, and Auger decays of the  $K^+ 3s^{-1}$  ( $^{1,3}S$ ) states.

A second objective of our work is to investigate post-collision interaction (PCI) in K  $3s$  photoionization. PCI is a well-known electron correlation effect which is observed in the vicinity of ionization thresholds: the slow photoelectron exchanges energy with the Auger electron in the presence of the ionic core [9]. PCI phenomena have been well documented in a variety of cases, see the reviews [9,10], and some selected examples of recent investigations [11–15]. However, usually, energies of the Auger electrons are much larger than the kinetic energies of the photoelectrons, and the PCI results mainly from the interaction of the photoelectron with the ionic field, which varies during the Auger decay. In the present case the kinetic energies of the Auger electrons are small ( $\sim 5$  eV) and we choose the photon energy to realize the condition that the energies of photoelectrons are close to those of the Auger electrons, so that the interaction between photoelectron and Auger electron cannot be neglected. Our objective is thus to probe the PCI phenomenon in this special configuration of low energy Auger electrons, and to test the validity of PCI models in this situation. In fact, the  $K^+ 3s^{-1}$  ( $^{1,3}S$ ) states can decay to two different electronic states, the  $K^{2+} 3p^{-1}4s^{-1}$  ( $^2P_{3/2}$ ) and ( $^2P_{1/2}$ ), which are separated by 268 meV [1]. The final state which is populated must be selected in order to define precisely the process under study. Experimentally this is done by a multielectron coincidence technique using a magnetic bottle time of flight spectrometer.

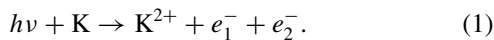
The paper is organized as follows: First, the principles of coincidence experiment will be recalled and its use in the present case will be explained. Then the properties of the inner valence  $K^+ 3s^{-1}$  ( $^{1,3}S$ ) states will be extracted from experiment, and

their lifetimes will be compared with predictions obtained from multiconfiguration Dirac-Fock calculations. The last part will be devoted to the evolution of the profiles of the Auger spectra as a function of the excess energy. Experimental profiles will be compared with predictions from the PCI theories.

## II. EXPERIMENT

The experiments were carried out at the SOLEIL synchrotron facility in Saint Aubin (France), on the undulator beamline PLEIADES [16]. Single bunch operation of the SOLEIL synchrotron provided light pulses every 1184 ns. A mechanical asynchronous chopper can be inserted in order to extend the light interval to 12.5  $\mu$ s [17]. The experimental setup is a 2-m-long magnetic bottle multielectron coincidence spectrometer, called HERMES (for a high energy resolution multielectron spectrometer). It is based on the design by Eland [18] and was described in detail in previous publications, to which the reader can refer (see [19] and references therein). Briefly, bunches of electrons produced in the multiple photoionization of a single atom by a pulse of light from the synchrotron are detected. The individual time of flight of electrons, with respect to the light pulse, are recorded by a time to digital converter with a 275 ps discretization step (“Isitime” developed at the LUMAT laboratory in Orsay France). Calibration and conversion from electron time of flights to kinetic energies were achieved by measuring photoelectron lines of He at different photon energies. The energy resolution  $\Delta E/E$  of the spectrometer was 1.6% for  $E > 1$  eV. Electron detection efficiencies were deduced from Ar  $2p^{-1}$  Auger-electron photoelectron coincidences and amount to  $70 \pm 5\%$  for electrons with energy less than 100 eV. Potassium vapor was created by a homemade resistively heated oven operated at  $\sim 190^\circ\text{C}$ . A liquid nitrogen trap was set in front of the oven to minimize pollution from K vapors.

Figure 1 shows the single and double photoionization spectra of the K atom, obtained at a photon energy of 44.5 eV. A mechanical chopper [17] was used to increase the light bunch interval and allows the absolute measurement of electron time of flights, which are limited to  $\sim 7 \mu$ s, due to the application of a weak electrostatic field in the source volume. Figure 1(a) shows the conventional photoelectron spectrum and reveals the unresolved  $3p^{-1}$  components and their satellites. The  $3s^{-1}$  photoelectrons and the associated Auger lines are barely distinguished above the background due to low energy electrons. The double ionization spectrum, shown in Fig. 1(b), is retrieved by detecting the two photoelectrons emitted in the double ionization process in coincidence:



The binding energy of the  $\text{K}^{2+}$  final state is obtained by energy conservation and by plotting in Fig. 1(b) the photon energy minus the sum of the kinetic energies of the two photoelectrons. We resolve here the two  $\text{K}^{2+}$  final states:  $3p^{-1}4s^{-1}$  ( ${}^2P_{3/2}$ ) and ( ${}^2P_{1/2}$ ). The comparison of the count rates in Figs. 1(a) and 1(b) gives directly the ratio of double to single photoionization. Taking into account the detection efficiencies we deduce a  $4 \pm 0.5\%$  value for the ratio of double photoionization to the single photoionization in the  $3p$  shell.

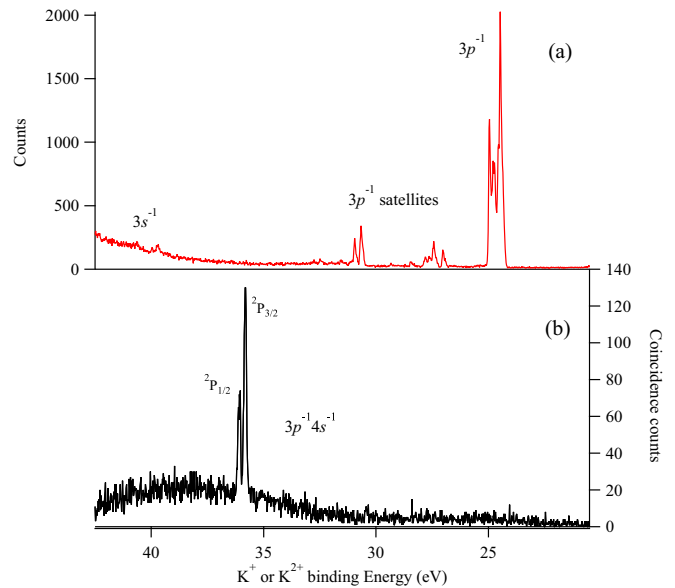


FIG. 1. (Color online) Spectra of single (a) and double (b) photoionization of K at a photon energy of 44.5 eV.

The energy correlation between the two photoelectrons in reaction (1) is represented in Fig. 2 by reporting the kinetic energy of the faster electron with respect to that of the slower one. Contrary to Fig. 1, these results were obtained without the light chopper [17] in order to gain photon intensity, which is crucial for low density species such as K vapors. The price to pay is that absolute electrons’ time of flight is no longer measured and that overlap between different processes may occur. In the present case it was essential to remove second order light contribution by the insertion of a 0.4  $\mu$ m thin Al filter. In its absence, spurious coincidence lines due to double ionization by second order photons of 91 eV would pollute the coincidence spectra and appeared at false locations due to their

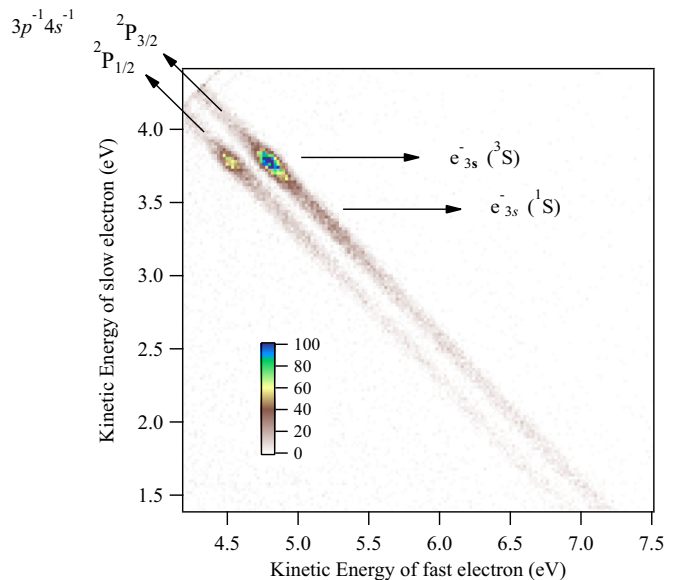


FIG. 2. (Color online) Energy correlation between the two electrons emitted upon double photoionization at  $h\nu = 44.5$  eV.

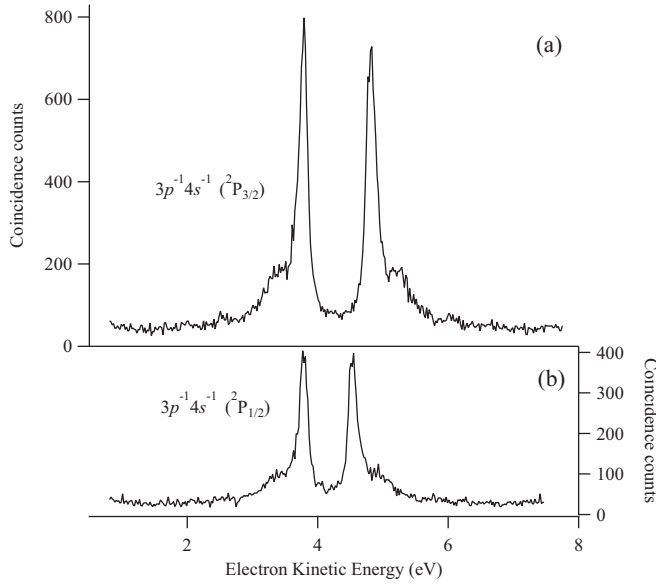
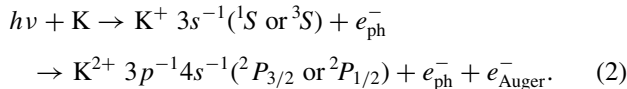


FIG. 3. Energy sharing between the two electrons emitted upon formation of the two  $K^{2+} 3p^{-1}4s^{-1}$  states: ( ${}^2P_{3/2}$ ) in (a) and ( ${}^2P_{1/2}$ ) in (b). Obtained from Fig. 2 (measured at  $h\nu = 44.5$  eV) as the intensities along the corresponding diagonal lines.

wrong time to energy conversion. In Fig. 2 two diagonal lines corresponding to the two  $K^{2+} 3p^{-1}4s^{-1}$  ( ${}^2P_{3/2}$ ) and ( ${}^2P_{1/2}$ ) final states are observed. A weak intensity along all the lines is associated with the direct double photoionization process, but the figure is dominated by intense spots. The spots correspond to an indirect process in which an electron from a  $3s$  inner valence shell is first ejected, leaving a  $K^+ 3s^{-1}$  stationary state, which Auger decays in a second step:



The energy sharing between the photoelectron and the Auger electron is given by the intensity along the diagonal lines in Fig. 2 and is reported in Fig. 3. The coincidence technique enables us to separate the  $K^{2+}$  final state:  $K^{2+} 3p^{-1}4s^{-1}$  ( ${}^2P_{3/2}$ ) in Fig. 3(a) and  $K^{2+} 3p^{-1}4s^{-1}$  ( ${}^2P_{1/2}$ ) in Fig. 3(b). Photoelectron peaks appear at the same kinetic energies in the two curves at around 3.7 eV, but Auger electrons are shifted, as determined by the energy difference between the two  $K^{2+}$  final states. The  $3s$  photoelectron peak is seen to be double with a thin main peak associated with the  $K^+ 3s^{-1}$  ( ${}^3S$ ) state and a broader component corresponding to the  $K^+ 3s^{-1}$  ( ${}^1S$ ) component, as will be detailed in Sec. III A. In this study we will observe the evolution of the Auger line shapes as a function of the excess energy, as a probe of the PCI effect. The coincidence method is very important for this study: it enables the separation of the Auger peaks as a function of the  $K^{2+}$  final state, while they would overlap in noncoincidence experiments.

Note that the energy distributions in Fig. 3 do not extend down to 0 eV as contact potential prevented detection of low energy electrons. The energy limit  $El$ , below which electrons are not detected, changes with experimental conditions, and it is observed to vary during the experiment on K vapors,

depending on the pollution of the surfaces by K deposition. In the conditions of Figs. 2 and 3,  $El$  was estimated at 0.8 eV, as deduced from the analysis of the lines in Fig. 2 that are observed (in the low energy range which is not presented in Fig. 2) to vanish for electron energies below 0.8 eV. Because electrons from reaction (1) are detected in pairs, absence of detection of the low energy electron in the pair implies necessary absence of the fast companion electron. For instance in Fig. 3(a) the distribution should extend up to  $E = 8.5$  eV ( $h\nu$  minus the binding energy of  $K^{2+}$  final state) but is effectively limited to  $E - El = 7.7$  eV. For the measurements presented in this paper, the polarization of the photons was set linear and vertical, and it was checked that the line shapes of the spectra were the same with the use of horizontal linear polarization.

### III. RESULTS AND DISCUSSION

#### A. Spectroscopy and lifetime of the $K^+ 3s^{-1}$ states

##### 1. Experimental characterization of the $K^+ 3s^{-1}$ states

In order to get spectroscopic information on the  $K^+ 3s^{-1}$  states we measured the high resolution photoelectron spectrum presented in Fig. 4. A Scienta SES-200 hemispherical analyzer was used at the Advanced Light Source (ALS) synchrotron radiation facility of the Lawrence Berkeley National Laboratory. More details on the experimental arrangement can be found in Cubaynes *et al.* [20]. The energy scale was calibrated with the  $K^+ 3s^2 3p^5 4s^1$  ( ${}^3P_2$ ) photoelectron line of 24.489 eV binding energy [1]. Figure 4 shows the two components of the  $K^+ 3s^{-1}$  photoelectron line. The photon energy was set at 100 eV in order to eliminate PCI effects. A fitting of the spectrum with the superposition of two Voigt profiles shows a combined photon plus analyzer resolution of 51 meV, and

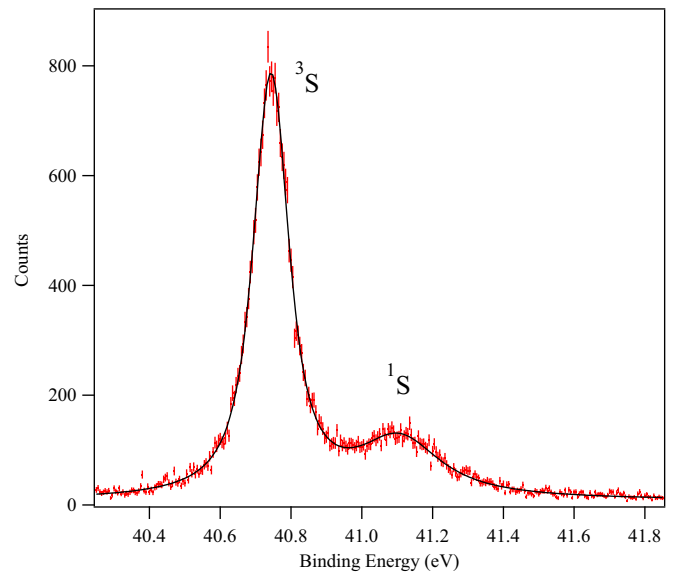


FIG. 4. (Color online)  $3s$  Photoelectron spectrum, measured at ALS with a Scienta analyzer showing the two spin-orbit components ( ${}^3S$ ) and ( ${}^1S$ ) of the  $K^+ 3s^{-1}$  photoelectron line. The spectrum was measured at  $h\nu = 100$  eV, and the lines were fitted with two Voigt profiles. It is presented as a function of the binding energy of the  $K^+$  states.

TABLE I. Characteristics of the  $3s^{-1}$  ( $^3S$ ) and ( $^1S$ ) states. Experimental results are deduced from Fig. 4. The present calculations use either the single configuration (SC) or multiconfiguration (MC) approach, see text.

State	Binding energy (eV)			Linewidth (meV)			Nominal Auger energy (eV)	
	Experiment	Calculation		Experiment	Calculation		to $K^{2+} 3p^{-1}4s^{-1}$ experiment	
		SC	MC		SC	MC	( $^2P_{3/2}$ )	( $^2P_{1/2}$ )
$3s^{-1}$ ( $^3S$ )	$40.742 \pm 0.005$	45.57	39.42	$97 \pm 11$	443	149	4.77	4.51
$3s^{-1}$ ( $^1S$ )	$41.100 \pm 0.005$	46.28	40.07	$287 \pm 29$	80	296	5.13	4.87

gives the binding energies and natural linewidths of the two  $K^+ 3s^{-1}$  components, which are reported in Table I. The nominal Auger energies (that is in the absence of PCI) are deduced from the  $K^{2+}$  binding energies [1].

It is observed that, similar to the Rb [3] and Cs [4] cases, the inner valence ionization in the  $ns$  shell leads to two states of very different lifetimes, the ( $^1S$ ) multiplet being almost three times shorter lived than the ( $^3S$ ) one. From their observation on Rb, Schultz *et al.* [3] proposed a simple explanation: the Auger transition rates from the  $Rb^+ 4s^1 4p^6 5s^1$  ( $^1^3S$ ) to the  $Rb^{2+} 4s^2 4p^5$  ( $^2P$ ) states include the contribution of the paths in which a  $5s$  electron decays into the  $4s$  hole while a  $4p$  electron is ejected. These transitions are more probable from the  $Rb^+$  singlet state, in which the spins of the  $4s$  and  $5s$  electrons are antiparallel. Instead, a less probable spin-flip process during the Auger decay is needed for the decay from the triplet state, implying a longer lifetime for this triplet state. Partanen *et al.* [4] showed that this simple explanation is not correct, as their single configuration Hartree-Fock calculation on Rb and Cs predicted the opposite trend for the singlet and triplet  $ns^{-1}$  states lifetimes. They showed instead that the configuration interaction between the  $5s^{-1}$  and  $5p^{-2}5d^1$  configurations is essential in predicting the correct lifetime broadenings. We performed here calculations for the K  $3s^{-1}$  states in order to compare with the Rb and Cs case and get a better insight into this phenomenon.

## 2. Calculations of the energies and linewidths of the $K^+ 3s^{-1}$

In order to simulate the experimental  $3s^{-1}$  photoelectron spectrum of K, first the binding energies of ground, single ionized and double ionized states of potassium were calculated with the multiconfiguration Dirac-Fock (MCDF) method. The radial wave functions of the one-electron spin-orbitals were obtained with the GRASP92 program [21] using the average level (AL) scheme for the optimization of the wave functions. The atomic state functions (ASFs) for bound states were obtained by diagonalizing the Hamiltonian matrix in the basis of JJ-coupled antisymmetric configuration state functions (CSFs) with RELCI component of the RATIP package. The linewidths of the ionized

states are calculated using the AUGER component from the RATIP [22–24].

The ground state of potassium was described with the single configuration (SC)  $[Ar]4s^1$  state. Binding energies and lifetimes for the  $3s^{-1}$  states were first calculated by using a basis set including the states belonging to the nonrelativistic configurations  $3s^1 3p^6 4s^1$  and  $3s^1 3p^6 3d^1$ . For the double ionized final states, the basis set including states from non-relativistic configurations  $3s^2 3p^5$ ,  $3s^2 3p^4$  ( $3d$ ,  $4s$ ,  $5s$ ) $^1$  was used. These calculations give the binding energies of the  $3s^{-1}$  states 5 eV too high and the linewidth 443 meV for the ( $^3S$ ) and 80 meV for the ( $^1S$ ) state, which are very far from the experimental values 97 meV for ( $^3S$ ) and 287 meV for the ( $^1S$ ) state.

In order to find a role of configuration interaction, MCDF calculation for  $3s^{-1}$  state was performed including the configurations  $3s^1 3p^6(3d, 4s, 4d, 5s)^1$ ,  $3s^2 3p^4(3d, 4s, 4d, 5s)^2$ ,  $3s^2 3p^4 3d 4d$ ,  $3s^2 3p^4 3d^1 ns^1$ , and  $3s^2 3p^4 4d^1 ns^1$ ,  $n = 4-5$ . The interaction between the configurations  $3s^1 3p^6 4s^1$  and  $3s^2 3p^4 4s^1 3d^1$  is found to be strong and it changes also the linewidth of the ( $^1S$ ) and ( $^3S$ ) states remarkably increasing the broadening of the singlet state and decreasing the broadening of the triplet state. The leading configurations of the states are given in Table II. When looking at the calculated binding energies against the experiment one observes that MCDF calculation improves the agreement, but leaves still an offset of about 1 eV. This could be accounted for by increasing the size of the CSF basis, but since the fourth configuration already comes to the ASF expansion with a weight of only 1%, the required increment would have to be dramatic.

CI interchanges the transition rates of the  $3s^{-1}$  multiplet states increasing the broadening of the singlet state to 296 meV and decreasing the broadening of the triplet state to 149 meV. However, the ( $^3S$ ) line remains still too broad in comparison with the experiment. In the study of Cs [4], configuration interaction (CI) between the  $5s^1 5p^6 6s^1$  and  $5s^2 5p^4 5d^1 6s^1$  configurations was also found to be essential in predicting the lifetime broadenings. The CI is strong between the states  $5s^1 5p^6 6s^1$  ( $^3S$ ) and  $5s^2 5p^4(1D)5d^1 6s^1$  ( $^3S$ ), and the Auger amplitudes of the ( $^3S$ ) components are found to be opposite

TABLE II. Leading configurations of the K  $3s^{-1}$  states from the MCDF calculations.

State	Configurations			
	$3s 3p^6 4s$	$3s^2 3p^4 3d 4s$	$3s^2 3p^4 4s 4d$	$3s 3p^6 5s$
$^3S$	63%	27%	7%	1%
$^1S$	62%	27%	8%	1%

in sign, so they partly cancel each other. This decreases the Auger transition rates of the ( $^3S$ ) state and makes the linewidth narrower. The singlet states is a combination of  $5s^15p^66s^1(^1S)$  and  $5s^25p^4(^1D)5d^16s^1(^1S)$  states. The Auger amplitudes of the ( $^1S$ ) components have equal signs and the Auger amplitude of  $5s^25p^4(^1D)5d^16s^1(^1S)$  is high, which also makes the  $5s^15p^66s^1(^1S)$  line broad. Although our present calculations do not identify the sign of the Auger amplitudes, the similarity of the K and Cs configurations indicates that the same reason causes the dramatic changes in the linewidths also in K. Although the MC calculation improves the predicted binding energies of the states, they are still more than 1 eV from the experimental value.

It is interesting to compare with the Na case: the lifetime broadenings of the equivalent  $2s^{-1}(^3S)$  and ( $^1S$ ) states are not reported in the literature, but have been estimated in a recent experiment to, respectively,  $245 \pm 5$  and  $202 \pm 6$  meV [25]. This is the reverse order of the other alkali-metal K, Rb [3], and Cs [4]. This difference illustrates nicely the effect of the CI between the  $ns^1np^6(n+1)s^1$  and the  $ns^2np^4nd^1(n+1)s^1$  configurations which obviously does not exist in Na ( $n = 2$ ).

### B. Effect of post-collision interaction on the $3s^{-1}$ Auger line shapes.

The effect of post-collision interaction on the  $3s^{-1}$  Auger decay has been investigated in the near threshold region. The results are presented in Figs. 5 and 6 which display the profiles of the Auger spectra at selected photon energies. Note that our method gives directly angle integrated electron spectra, which correspond to the electron emission over the entire  $4\pi$  solid angle. Figure 5 displays the decay of the  $3s^{-1}(^1,^3S)$  states to the  $K^{2+} 3p^{-1}4s^{-1}(^2P_{3/2})$  state while for Fig. 6 it is to the  $K^{2+} 3p^{-1}4s^{-1}(^2P_{1/2})$  state. The experimental procedure is the same as explained in the Experiment section. At the higher photon energy (48 eV) photoelectrons (of  $\sim 7$  eV) are faster than the Auger electrons, contrary to the other three spectra which correspond to excess energies of around 1, 2, and 3.5 eV.

#### 1. Theoretical description of the PCI distorted Auger spectra

The PCI is known as a Coulomb interaction between emitted charged particles in the intermediate and final states when the reaction occurs in two stages via an intermediate resonance. In the present case, which is described by reaction (2), and more generally for inner shell photoionization processes, the PCI reduces to the interaction between the slow photoelectron and the ionic field which varies during the Auger decay as well as to the interaction between the photo- and Auger electrons [9]. The PCI distortion depends on the width  $\Gamma$  of the inner vacancy and on the energies and the angle directions of the emitted electrons, i.e., on the kinematics of the process.

There are two characteristics of the PCI investigation in our case of the K  $3s$  photoionization.

First, we consider the emission of low energy photoelectrons, of a few eV, followed by single Auger decay with emission of Auger electrons with energies of close to 5 eV. Usually the main contribution to the PCI in near threshold region comes from the interaction of slow photoelectron with the ion field. But in our case the interaction between the

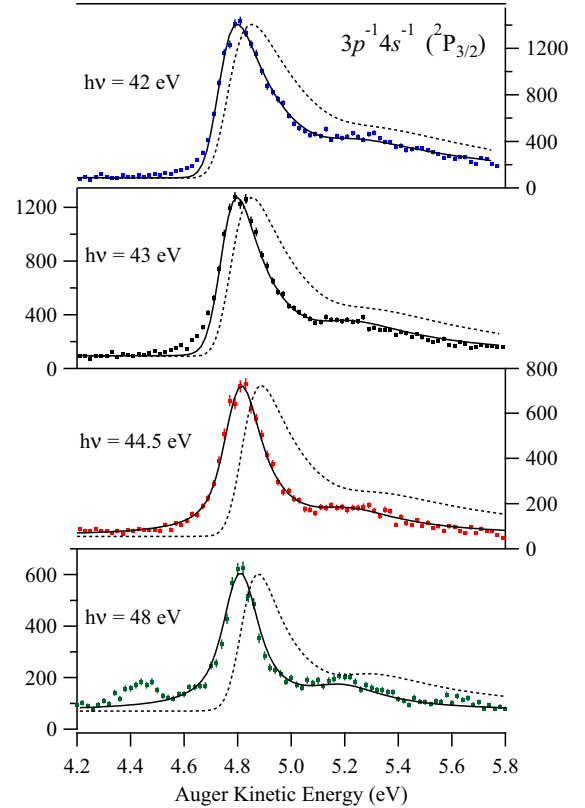


FIG. 5. (Color online) Auger spectra for decay of the  $3s^{-1}(^1,^3S)$  states to the  $3p^{-1}4s^{-1}(^2P_{3/2})$  final states. The spectra show the experimental evolution of the PCI profile with excess energy (bars) and compares them to our calculations (full line); the dotted line present the calculated hypothetical PCI profile in the absence of electron-electron interaction (see text). The sharper peak corresponds to the Auger electrons emitted in the decay of the longer lived  $3s^{-1}(^3S)$  state, while the broader component at higher kinetic energy comes from the Auger decay of the shorter lived  $3s^{-1}(^1S)$  state.

photo- and Auger electrons contributes also notably, because their energies are of the same order of magnitude. These contributions can be estimated with the help of the eikonal approach to the PCI description [26]. According to this model the PCI influence is governed by the parameter  $\xi$ ,

$$\xi = \frac{1}{V_{\text{ph}}} - \frac{1}{|V_{\text{ph}} - V_{\text{Aug}}|}, \quad (3)$$

where  $V_{\text{ph}}$  and  $V_{\text{Aug}}$  are, respectively, the velocities of the photo- and Auger electrons. The first term in parameter  $\xi$  reflects the interaction of the photoelectron with the ion field and the second one is associated with the interaction between the photo- and Auger electrons. It is seen that these terms have opposite signs and for some kinematics, which are present in our measurements, they can compensate each other. Hence we cannot expect a monotonic behavior of the PCI shift that is typical for the near threshold region. Moreover, we need to take into account accurately all the interactions between the emitted particles within the models which we apply to calculate the photoelectron's energy distribution. The eikonal approach [26] is based on the assumption that the kinetic energy  $W_{\text{kin}}$  is much greater than the potential energy  $W_{\text{pot}}$  of

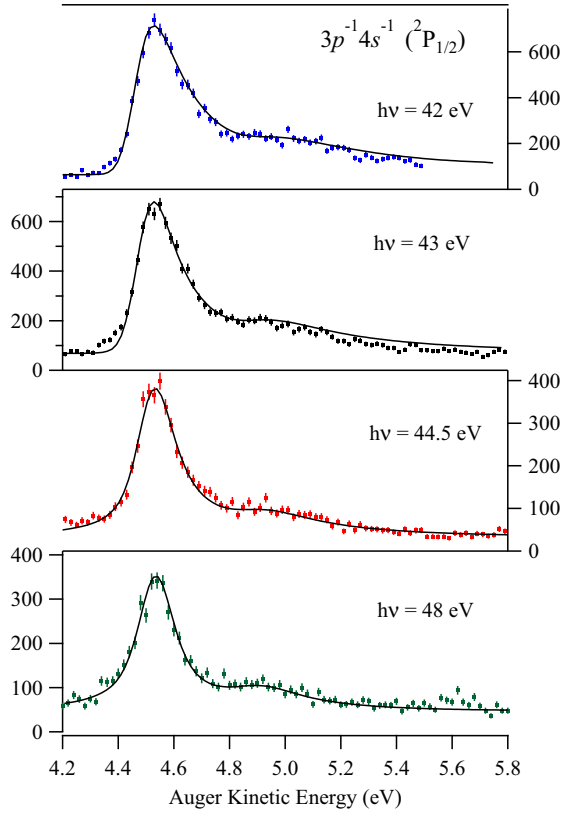


FIG. 6. (Color online) Same as in Fig. 5 but for the decay to  $K^{2+} 3p^{-1}4s^{-1}(^2P_{1/2})$  final states.

the interacting particles:  $W_{\text{kin}} \gg W_{\text{pot}}$ . This condition leads to a limitation for the energies of the slow photoelectron  $E_{\text{ph}} : E_{\text{ph}} \gg \Gamma^{2/3} (E_0/2)^{1/3}$ , where  $E_0$  is the atomic unit of energy. It is seen that this condition breaks down for very low energies of the emitted photoelectrons (for example, for the excess photon energy of 1 eV above the threshold the left and right sides of this inequality are, respectively, equal to 0.037 and 0.0185) and the eikonal approach cannot be used in this case for the correct calculation. Using the eikonal model in this energy region leads to a notable difference in the line shapes, compared to the experiment and to more adequate models, as was investigated in a recent work [27]. On the other hand the semiclassical model of the PCI [28] describes adequately all the interactions in the near threshold region and we will use this approach to calculate the energy distributions for the photon energies 42 and 43 eV, i.e., photoelectron energies of  $\sim 1-2$  eV. However, the semiclassical method has also a restriction, which is  $0 < \frac{V_{\text{ph}}}{|V_{\text{ph}} - V_{\text{Aug}}|} < 1$  (see [28]). For the photon energies 44.5 and 48 eV the energies of the photoelectrons are close to 3.5 and 7 eV, respectively, whereas the energy of the Auger electron is close to 5 eV. Hence this condition breaks down for some kinematics and the semiclassical model cannot be used for calculation of the cross sections in such kinematical conditions. An elimination of these events from the integration over the emission angles can lead to some error because of large phase volume of these kinematics. Therefore, for the reliability of calculations at the photon energies 44.5 and 48 eV, we have used the eikonal approach, taking an exact account of the interaction between emitted electrons [29].

The second feature of our PCI investigation is that there are two intermediate states  $3s^{-1}(^3S)$  and  $3s^{-1}(^1S)$  of the  $K^+$  ion which can Auger decay to the same final  $K^{2+}$  ionic state,  $K^{2+} 3p^{-1}4s^{-1}(^2P_{3/2}$  or  $^2P_{1/2})$ . The energy difference between these  $3s^{-1}$  states is small, 0.36 eV, and both Auger electrons from the decay of the ( $^3S$ ) and ( $^1S$ ) states contribute to the measured Auger-electron energy distribution. Note that these electrons contribute incoherently to the Auger-electron spectrum because of different spin states of the emitted photoelectron and one needs to sum the cross sections of the different Auger-electrons emission [from ( $^3S$ ) and ( $^1S$ ) states] to describe correctly the measured energy distribution. Another important feature of our case is the different widths  $\Gamma$  of the intermediate ( $^3S$ ) and ( $^1S$ ) states which are 97 and 287 meV, respectively. Because the PCI distortion depends on the width  $\Gamma$ , the line shapes are expected to be rather different depending on the photon energy. So the angular dependent cross section for the Auger electrons yield can be calculated according to the equation

$$\frac{d\sigma}{dE}(\theta) = \frac{d\sigma(^3S)}{dE}(\theta) + R \frac{d\sigma(^1S)}{dE}(\theta). \quad (4)$$

Here  $\frac{d\sigma(^3S)}{dE}$  and  $\frac{d\sigma(^1S)}{dE}$  are, respectively, the differential cross sections for the Auger-electrons yield from the decay of ( $^3S$ ) and ( $^1S$ ) states. These cross sections take into account the PCI distortion and are calculated within the semiclassical approach [28] (for the photon energies 42 and 43 eV) or within the eikonal model [29] (for the photon energies 44.5 and 48 eV). The factor  $R$  takes into account the relative contribution of the ( $^3S$ ) and ( $^1S$ ) states. Because our measurements do not fix the angle  $\theta$  between the directions of the electron emission the cross section (4) has to be integrated over the angle  $\theta$ , and it has been done in our calculations.

## 2. Comparison of experimental and theoretical PCI profiles

In order to compare the calculated Auger PCI profiles (full lines) with the experimental ones (Figs. 5 and 6), we adopted the following procedure. The calculated curves have been convoluted with a Gaussian function of 80 meV FWHM in order to take into account the experimental resolution. In a first step we have calculated in our eikonal model, the shape of the photoelectron line at a photon energy near 100 eV and compared it both with measurements and with the simple Voigt profiles used in Fig. 4. We obtain good agreement which confirms the absence of PCI distortion at this excess energy, and the values of 97 and 287 meV presented in Table I, for the widths of ( $^3S$ ) and ( $^1S$ ) states, respectively. This is a critical parameter as our calculations are very sensitive to the choice of widths of the ( $^3S$ ) and ( $^1S$ ) states. Apart from this, the comparison with the measurements allows us to estimate the value of the factor  $R$  [see Eq. (4)] which takes into account the relative contribution of the two  $3s^{-1}(^3S, ^1S)$  states to the total Auger-electron emission. We obtain  $R = 0.4$  in the conditions of Fig. 4. For the calculations of the Auger spectra in Figs. 5 and 6, the ratios  $R$  were adjusted at each photon energy and found to increase slowly with photon energy (with values  $R$  of, respectively, 0.3, 0.3, 0.35, and 0.4 for photon energies of 42, 43, 44.,5 and 48 eV). Note that our measured  $R$  values are close to the ones calculated by Kupliauskienė [8], who

predicted at 50 eV values of 0.23 or 0.39 depending on their MCHF or HF approach, and suggested also a photon energy dependence for  $R$  in the threshold region. The maxima of our theoretical curves have been normalized to the experimental ones, while allowing for a small uniform background assigned to direct double photoionization. An extra peak is observed at 4.45 eV in Fig. 5 for the measurement at 48 eV photon energy. We assign it to a photoelectron peak and the formation of a  $K^+ 3s^{-1}$  satellite state of 43.6 eV binding energy and probable  $K^+ 3s^1 3p^6 4p^1$  configuration. The same photoelectron may also pollute the spectrum taken at 48 eV in Fig. 6, and be at the origin of the broadening of the Auger peak on its low energy side.

The agreement between experiment and calculations (full lines) in Figs. 5 and 6 is found to be very good and validates the PCI models that we have used. A small disagreement in Fig. 6 on the high energy side for the photon energy 43 eV can be attributed to the overestimated value of the parameter  $R = 0.300$ . Note that we have used in calculation the same values of  $R$  for both transitions to the  $^2P_{3/2}$  and the  $^2P_{1/2}$  final states and probably the value of  $R$  is slightly less for the latter case. We observe a strong distortion of the Auger lines, especially at lower photon energy. As expected, distortion is more important for the decay of the shorter lived  $3s^{-1}(^1S)$  state, which gives the broad peak at higher kinetic energy. PCI distortion prevents the separation of the ( $^1S$ ) and ( $^3S$ ) contributions which appear to merge at 42 and 43 eV photon energies, but are clearly distinguished in the absence of PCI in Fig. 4 and at 48 eV. Note that the coincidence method is here essential to separate the four possible Auger components and filter them according to the  $K^{2+}$  final state. Without this method, the curves in Figs. 5 and 6 would be summed up and it would be difficult to evidence the detail of the shapes of the Auger lines. There are two interesting points in this specific configuration of PCI involving low energy Auger electrons: First, while distortion of the peaks is notable, the shift of the maximum of the PCI profile is weak. The calculations predict that the sharper Auger peak due to the decay of the  $3s^{-1}(^3S)$  state shifts, respectively, by 100, 70, and 20 meV at 42, 43, and 44.5 eV, compared to its value at 48 eV photon energy where PCI distortion is observed to be weak. Due to the limited experimental resolution of 80 meV, this predicted limited shift is in reasonable agreement with the experiment which suggests a value of around 50 meV at 42 eV. Second, as noted above, we are in special conditions where the low energy Auger electrons ( $\sim 4.8$  eV) have kinetic energies comparable to the photoelectrons (nominal energies of  $\sim 1.3, 2.3, 3.8,$  and  $7.3$  eV here), and we expect the influence of the direct interaction between the photo- and the Auger electron. In order to test this effect we have calculated what would be the PCI distortion in the absence of direct interaction between the photoelectron and the Auger electron. The result is represented by the dotted lines in Fig. 5 for the case of the decay to the  $K^{2+} 3p^{-1} 4s^{-1}(^2P_{3/2})$  state. Similar results and conclusions would be obtained for the decay to the  $K^{2+} 3p^{-1} 4s^{-1}(^2P_{1/2})$  state in Fig. 6. The comparison between the calculated PCI profiles with (full line) and without (dotted lines) including this electron–Auger-electron interaction demonstrates clearly its importance. It is seen that taking into account the electron–electron interaction has the

effect to reduce the calculated peak width and to decrease the shift of the line maximum in agreement with experimental results, in other words, to decrease the PCI distortion. This effect comes from the fact that the photoelectron–Auger interaction contributes with an opposite sign compared to the interaction of the photoelectron and the ionic core, see the parameter  $\xi$ , see Eq. (3), and partially cancels its effect. As expected, the effect is stronger when the photoelectron and Auger electrons have the closest energies (spectrum at 44.5 eV). A strong effect is also observed at 48 eV photon energy although the photoelectron is then faster than the Auger electron. This demonstrates the quantum nature of the PCI effect, as a classical nonpassing model would not predict PCI distortion. According to a classical picture, the PCI effect occurs solely when the fast Auger electron overtakes the slow photoelectron and the slow photoelectron “feels” the change of the ionic field. Note that another example of the influence of the direct interaction between the photo- and the Auger electron in PCI during single Auger decay, was given in the study of the Xe  $4d$  Auger decay [30]. The effect is stronger in the present case as the kinetic energies of the Auger electron and of the photoelectron are lower and closer to each other.

#### IV. CONCLUSIONS

Ionization in the inner valence  $3s$  shell of K atoms was investigated using synchrotron radiation. The spectroscopy and lifetime widths of the  $3s^{-1}(^1S)$  and ( $^3S$ ) states were extracted from conventional photoelectron spectra, obtained with a Scienta analyzer at ALS. The lifetime of the ( $^3S$ ) component is found to be significantly longer than that of the ( $^1S$ ) one (widths of 97 versus 287 meV). Calculations demonstrate that, similar to the Rb ( $4s$ ) and Cs ( $5s$ ) equivalent cases [3,4], the description of the intermediate  $3s^{-1}$  states with a single configuration leads to a reverse order for the lifetimes. The origin of the observed lifetimes comes from electron correlation effects and the influence of the unoccupied  $3d$  orbital. Especially it is important to use a CI description of the  $3s^{-1}$  states and include the mixing between the  $3s^1 3p^6 4s^1$  and  $3s^2 3p^4(^1D) 3d^1 4s^1$  configurations. The subsequent Auger decay of the  $3s^{-1}(^1S)$  and ( $^3S$ ) states was then observed with a multielectron coincidence technique based on a magnetic bottle time of flight spectrometer. This method allows the separation of the Auger spectra according to the  $K^{2+}$  final state and a clear definition of the process under study. It is particularly well suited to investigate the near threshold region where PCI effects are observed. The PCI profiles of the Auger peaks are well reproduced by adequate PCI models. They demonstrate that in these specific case where low energy Auger electrons ( $\sim 5$  eV) are involved, the weak PCI shift and strong PCI distortion are influenced not only by the Coulomb interaction of the photoelectron with the ion core, but also by the direct interaction of the photoelectron and the Auger electron. Note that the present results are angle integrated, and that stronger effects are expected for instance when both electrons are emitted in the same direction. It would be interesting to probe this effect with a more sophisticated angle-resolved setup such as a reaction microscope or a COLTRIMS apparatus.

## ACKNOWLEDGMENTS

The experiment was performed at SOLEIL Synchrotron (France) at the PLEIADES beamline, with the approval of the Soleil Peer Review Committee (Projects No. 20120132 and No. 20131019). We are grateful to M. Patanen, C. Nicolas, C. Miron, and the PLEIADES team for help during the measurements and to SOLEIL staff for stable operation of the storage ring. We thank John Bozek, Norra Berrah, Sophie Canton, Eugene Kennedy, and Francois Wuilleumier for their

help in the measurements of the K3s photoelectron spectrum at ALS. K.I. acknowledges the support of the Labex Plas@Par managed by the Agence Nationale de la Recherche, as part of the “Programme d’Investissements d’Avenir” under Reference No. ANR-11-IDEX-0004-02. This work has been financially supported by the Research Council for Natural Sciences and Engineering of the Academy of Finland. The Väisälä Foundation is acknowledged by S.-M. H. EXACTUS-DP (Doctoral Program in Exact Sciences) is acknowledged by J.S.

- 
- [1] A. Kramida, Yu. Ralchenko, J. Reader, and NIST ASD Team (2014), *NIST Atomic Spectra Database* (ver. 5.2) [Online]. Available:<http://physics.nist.gov/asd> [February 11, 2015], National Institute of Standards and Technology, Gaithersburg, MD.
- [2] M. Richter, J. M. Bizau, D. Cubaynes, T. Menzel, F. J. Wuilleumier, and B. Carré, *Europhys. Lett.* **12**, 35 (1990).
- [3] J. Schulz, E. Loos, M. Huttula, S. Heinäsmäki, S. Svensson, S. Aksela, and H. Aksela, *Europhys. Lett.* **83**, 53001 (2008).
- [4] L. Partanen, J. Schulz, M. Holappa, H. Aksela, and S. Aksela, *Phys. Rev. A* **80**, 042518 (2009).
- [5] M. Koide, F. Koike, Y. Azuma, and T. Nagata, *J. Electron Spectrosc. Relat. Phenom.* **144-147**, 55 (2005).
- [6] P. N. Juranić, J. Nordberg, and R. Wehlitz, *Phys. Rev. A* **74**, 042707 (2006).
- [7] H. Aizawa, K. Wakiya, H. Suzuki, F. Koike, and F. Sasaki, *J. Phys. B* **18**, 289 (1985).
- [8] A. Kupliauskiene, *J. Phys. B* **30**, 1865 (1997).
- [9] M. Yu. Kuchiev and S. A. Sheinerman, *Sov. Phys.-Usp.* **32**, 569 (1989).
- [10] V. Schmidt, *Rep. Prog. Phys.* **55**, 1483 (1992).
- [11] A. L. Landers, F. Robicheaux, T. Jahnke, M. Schoffler, T. Osipov, J. Titze, S. Y. Lee, H. Adaniya, M. Hertlein, P. Ranitovic, I. Bocharova, D. Akoury, A. Bhandary, Th. Weber, M. H. Prior, C. L. Cocke, R. Dorner, and A. Belkacem, *Phys. Rev. Lett.* **102**, 223001 (2009).
- [12] S. Sheinerman, P. Lablanquie, F. Penent, Y. Hikosaka, T. Kaneyasu, E. Shigemasa, and K. Ito, *J. Phys. B* **43**, 115001 (2010).
- [13] L. Gerchikov and S. Sheinerman, *Phys. Rev. A* **84**, 022503 (2011).
- [14] R. Guillemin, S. Sheinerman, C. Bomme, L. Journal, T. Marin, T. Marchenko, R. K. Kushawaha, N. Trcera, M. N. Piancastelli, and M. Simon, *Phys. Rev. Lett.* **109**, 013001 (2012).
- [15] Y. Hikosaka, M. Sawa, M. Nakano, K. Soejima, P. Lablanquie, F. Penent, and K. Ito, *J. Chem. Phys.* **138**, 214308 (2013).
- [16] J. Bozek *et al.*, <http://www.synchrotron-soleil.fr/portal/page/portal/Recherche/LignesLumiere/PLEIADES> and X. J. Liu, Q. Miao, F. Gel'mukhanov, M. Patanen, O. Travnikova, C. Nicolas, H. Ågren, K. Ueda, and C. Miron, *Nat. Photon.* **9**, 120 (2015).
- [17] K. Ito, F. Penent, Y. Hikosaka, E. Shigemasa, I. H. Suzuki, J. H. D. Eland, and P. Lablanquie, *Rev. Sci. Instrum.* **80**, 123101 (2009).
- [18] J. H. D. Eland, O. Vieuxmaire, T. Kinugawa, P. Lablanquie, R. I. Hall, and F. Penent, *Phys. Rev. Lett.* **90**, 053003 (2003).
- [19] J. Palaudoux, S.-M. Huttula, M. Huttula, F. Penent, L. Andric, and P. Lablanquie, *Phys. Rev. A* **91**, 012513 (2015).
- [20] D. Cubaynes, M. Meyer, A. N. Grum-Grzhimailo, J.-M. Bizau, E. T. Kennedy, J. Bozek, M. Martins, S. Canton, B. Rude, N. Berrah, and F. J. Wuilleumier, *Phys. Rev. Lett.* **92**, 233002 (2004).
- [21] F. A. Parpia, C. F. Fischer, and I. P. Grant, *Comput. Phys. Commun.* **94**, 249 (1996).
- [22] S. Fritzsche, *Comput. Phys. Commun.* **183**, 1525 (2012).
- [23] S. Fritzsche, *Phys. Scr.* **T100**, 37 (2002).
- [24] S. Fritzsche, *J. Electron Spectrosc. Relat. Phenom.* **114**, 1155 (2001).
- [25] D. Cubaynes (private communication).
- [26] M. Yu. Kuchiev and S. A. Sheinerman, *ZhETF* **90**, 1680 (1986) [*JETP* **63**, 986 (1986)].
- [27] Q. Wang, S. Sheinerman, and F. Robicheaux, *J. Phys. B* **47**, 215003 (2014).
- [28] P. van der Straten, R. Morgenstern, and A. Niehaus, *Z. Phys. D* **8**, 35 (1988).
- [29] M. Yu. Kuchiev and S. A. Sheinerman, *J. Phys. B* **21**, 2027 (1988).
- [30] S. A. Sheinerman, P. Lablanquie, F. Penent, J. Palaudoux, J. H. D. Eland, T. Aoto, Y. Hikosaka, and K. Ito, *J. Phys. B* **39**, 1017 (2006).